Applied Surface Science 478 (2019) 412–416

Contents lists available at ScienceDirect

Applied Surface Science

journal homepage: www.elsevier.com/locate/apsusc

Full length article

Infrared-laser precipitation of Dy^{3+}-Yb^{3+} codoped SrF_2 nanocrystals in glass and upconversion luminescence

Gangseon Ji[a], Gi-joon Hong[a], Chang-hyuck Bae[a], Palamandala Babu[b], Ki-Soo Lim[a,*]

[a] Department of Physics, Chungbuk National University, Cheongju 28644, Republic of Korea
[b] Department of Physics, SVCR Govt. Degree College, Palamaner 517408, India

ARTICLE INFO

Keywords:
SrF_2
Nanocrystals
CO_2 laser
Dy
Yb
Upconversion

ABSTRACT

Oxyfluoride glass-ceramics containing SrF_2nanocrystals have been prepared by a CO_2 laser treatment on the glass prepared by high temperature melt quenching. The optimized scan speed and laser power produced nanocrystals with sizes of ~10 nm. Energy dispersive spectroscopy mapping analysis showed that Dy^{3+} and Yb^{3+} ions are highly populated inside the SrF_2 nanocrystals. We also report a substantially enhanced down-converted visible emission from the 4F9/2 state of Dy3+ ions, including some violet emissions from the higher energy states under 365 nm excitation in the glass-ceramics, as compared to the as-made glass. Moreover, 980 nm laser diode excitation produced strong green and red emissions from the $^4I_{15/2}$ state and blue and yellow emissions from the $^4F_{9/2}$ state. A model has been proposed to interpret the upconversion emissions through the multistep-excitation of Dy^{3+} ions and energy transfers from, efficient sensitizers, Yb^{3+} ions to Dy^{3+} ions.

1. Introduction

Rare-earth ion doped glass-ceramics may become potentially useful for optoelectronic applications. Glass-ceramics offer the ease of melt processing like conventional glasses, but rare earth ion segregation to crystalline regions results in spectral and laser properties similar to those of single crystals and ceramics [1]. Oxyfluoride glass-ceramics have attracted much attention due to their combined advantages of oxide glasses and fluoride glasses [2,3] and their maintenance of good chemical and thermal stabilities [4]. Thus, numerous studies on oxyfluoride glass-ceramics containing fluoride nanocrystals doped with rare-earth ions have been reported thus far [3,5–8]. Fluoride nanocrystals have much less phonon energy (~360 cm^{-1}) [9], yielding a large quantum efficiency.

Most oxyfluoride glass-ceramics are fabricated using controlled heat treatments in an electric furnace in order to form nanocrystals in the interior of glass [10]. Recently, the laser annealing of glass has been reported as an alternative method for glass-ceramics formation with the advantage of spatially selected structural modification and crystallization inside glass with ultraviolet, visible, near-infra-red, and mid-infrared lasers [5,11–13]. Laser-heated glass-ceramics formation with an infrared laser hold some potential for optical device applications of oxyfluoride glasses with fluoride nanocrystals, because the infrared laser can treat selective regions upon the surface of the glass.

The infrared-to-visible up-conversion behavior of the glass-ceramics codoped with (Yb, Er) [14], (Yb, Tm) [15], (Yb, Ho) [16], or (Yb, Eu) [17] prepared by furnace treatment has been recently reported for display and solar-cell applications [18]. However, only a few studies on glass-ceramics co-doped with (Yb, Dy) have been reported thus far [19], and the blue-violet emissions still need further investigation before their origin can be clarified. Dy^{3+} ion exhibits intense blue and yellow colors as well as white light emission, and Yb^{3+} ions are widely used in infrared-to-visible upconversion applications [20]. In this work, CO_2 laser-induced crystallization technique has been used to a multi-component SiO_2-Al_2O_3-SrF_2-LiF oxyfluoride glass doped with rare-earth ions prepared by the melt-quenching process [15]. We report the precipitation of spatially selective glass-ceramics containing SrF_2 nanocrystals doped with Dy^{3+} and Yb^{3+} ions, as well as the enhancements of down-conversion and upconversion emissions of Dy^{3+} ions. The optimized conditions were achieved for emission enhancement by controlling the power and scan speed of the laser beam.

2. Experimental

The nominal composition of precursor glass (as-melted) used in this study was $40SiO_2$-$12Al_2O_3$-$23SrF_2$-24LiF-$0.5Yb_2O_3$-$0.5Dy_2O_3$ (mol.%). The raw materials used for preparation were fine grained powders from high purity (3 N) commercial chemicals. The starting batches were

* Corresponding author.
E-mail address: kslim@chungbuk.ac.kr (K.-S. Lim).

https://doi.org/10.1016/j.apsusc.2019.01.272
Received 7 September 2018; Accepted 29 January 2019
Available online 30 January 2019
0169-4332/

thoroughly mixed and melted at 1450 °C for 1 h in a covered platinum crucible under normal atmosphere. The melt was then cast into an iron mold prior to being annealed at 530 °C for 10 h, in order to release inner stress. Finally, the glass was cut and polished into the glass samples with a thickness of 1 mm. For thermal treatment to induce SrF_2 nanocrystals, we used a CO_2 laser employing various powers ranging from 0.9 to 1.3 W and scan speeds ranging from 0.1 to 0.3 mm/s.

The samples studied here are glass-ceramics prepared by the laser treatments of 1.3W_0.3 mm/s, 1.3 W_0.2 mm/s, 1.3W_0.1 mm/s, or 0.9W_0.3 mm/s, denoted by G1, G2, G3, and G4, respectively. The laser beam was focused on the surface of the glass. The selective area had a ~100 μm diameter. We employed micro-x-ray diffraction (μ-XRD, D/MAX RAPID-S) analysis for the irradiated regions in order to examine the formation of SrF_2 crystals. Furthermore, in order to clarify the size and crystallization of nanocrystals, we performed transmission electron microscopy (TEM, Titan G2 60-300) and EDS (Energy Dispersive Spectroscopy) analysis for the laser-treated surface. Photoluminescence and upconversion emission spectra for Dy^{3+} ions under 365 nm LED and 980 nm LD excitations were measured respectively for both unirradiated and irradiated glass area in order to confirm whether the ions are doped inside the nanocrystals.

3. Results and discussion

Micro- x-ray diffraction patterns of the glasses exposed to CO_2 laser with 0.3 mm/s scan speed and 1.3 W and 0.9 W powers (GC1 and GC4) are shown in Fig. 1, indicating the diffraction pattern of SrF_2 crystalline phase [21]. The XRD peaks were observed only in the CO_2 laser exposed area. The sharp and relatively intense peaks of the exposed area of glass can easily be assigned to the diffractions from the (111), (200), (220), (311), (222), (400), (331), and (420) planes of spinel SrF_2 phase (JCPDS No. 06-0262). This implies that the treated volume of the glass by CO_2 laser irradiation was changed into glass-ceramic. Although the x-ray beam has a slightly smaller size than the laser beam of ~100 μm on the surface and penetrates through the sample, the laser thermal treatment is only effective on the surface because of the low thermal conductivity of glass.

The average size of the nanocrystals has been calculated using the Scherrer formula [22] for XRD data of the lattice plane (*hkl*), using the full width at half maximum β, diffraction angle θ, and x-ray wavelength λ,

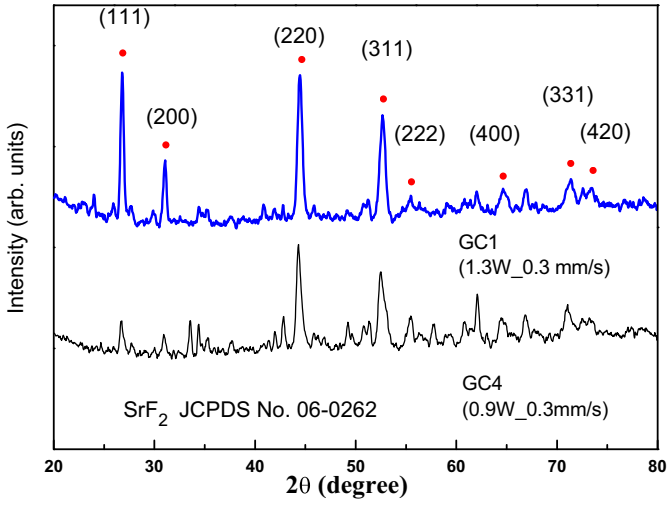

Fig. 1. XRD patterns of SrF_2 nanocrystals precipitated in glass by CO_2 laser irradiation with the power of 1.3 and 0.9 W (GC1 and GC4) and the same scan speed of 0.3 mm/s.

$$D(hkl) = \frac{0.9\lambda}{\beta \cos\theta} \quad (1)$$

The sizes of nanocrystals obtained with GC1 and GC4 are estimated at 15 and 13 nm, respectively. This implies that the laser thermal energy increases the sizes of the nanocrystals. The increase of XRD peaks indicates the increased density of nanocrystals in the glass. This implies that with increase in laser exposure time nucleation continues and the volume concentration of crystalline SrF_2 increases. In the TEM image of Fig. 2(a), the round-shaped nanocrystal with a size of ~300 nm can observed, with the background corresponding to the glassy phase. It is not a single domain, but seems to consist of many nanocrystals. In order to confirm the crystalline phases, high-resolution transmission electron microscopy (HRTEM) was employed. The HRTEM image in Fig. 2(b), which was collected by focusing an electron beam on the dark domain of Fig. 2(a), shows a well-defined lattice structure of the SrF_2 crystal with random orientation. The average size of nanocrystals is about 8 nm, which is smaller than the estimated value obtained from the Scherrer equation. A large temperature gradient in the laser-treated region originates from the inhomogeneous thermal distribution due to the use of the Gaussian laser beam. It produces various sizes of nanocrystals depending on the position [23]. Thus, the CO_2 laser irradiation energy was not sufficient to grow large nanoparticles of a single domain. Thus, we suggest that the larger crystallite size in Fig. 2(a) is due to the aggregation of nanocrystals.

The spatial distributions of Sr, F, Dy, and Yb ions are verified by EDS, as shown in Fig. 2(c)–(f), respectively. Fig. 2(c) and (d) show a large portion of Sr and F ions in the crystal displayed in Fig. 2(a), revealing the formation of SrF_2 crystal. It has been reported that the real fluorine concentration is somewhat lower than the nominal one, owing to the volatility of fluoride components at high temperature and the escape of fluorine from the melt [24]. Thus, a relatively low concentration of fluorine ions is expected as compared their initial doping concentration. Dy and Yb ions are located in the SrF_2 crystal domain as well as on the surface of the crystallites. The absorption spectrum of the glass in Fig. 3 shows the absorption peaks of Dy^{3+} and Yb^{3+} ions, implying that both ions have the absorption at 980 nm.

The emission spectra in Fig. 4 are obtained under 365 nm excitation reaching the $^6P_{5/2}$ state of Dy^{3+} ion. Laser heating could help to populate the $^6P_{7/2}$ state. The dominant blue (482 nm) and yellow (574 nm) bands are attributed to the transitions from the excited state of $^4F_{9/2}$ to the lower states of $^6H_{15/2}$ and $^6H_{13/2}$, respectively. Beyond that, we also observed weak emissions at 409, 418, 430, 445, 456, 660, and 725 nm, which correspond to $^6P_{7/2}$–$^6H_{13/2}$, $^6P_{5/2}$–$^6H_{11/2}$, $^4G_{11/2}$–$^6H_{15/2}$, $^4I_{13/2}$–$^6H_{13/2}$, $^4I_{15/2}$–$^6H_{15/2}$, $^4F_{9/2}$–$^6H_{11/2}$, and $^4F_{9/2}$–$^6H_{9/2}$ transitions from the glass-ceramics. Most of these violet emissions have not been reported under ultraviolet excitation for Dy^{3+} and Yb^{3+} co-doped glass or phosphors [25,26] because of the nonradiative relaxation from the $^6P_{5/2}$ and $^6P_{7/2}$ excited state to the $^4F_{9/2}$ state. This is further evidence for the emissions from nanocrystals doped with Dy^{3+} ions. The relatively strong blue and yellow emission intensities increased with laser exposure in the glass-ceramics (from GC1 to GC3). The GC3 shows more than 17 times enhancement of the overall visible emissions as compared to those from the untreated glass. The increase in emission intensities with laser exposure is evidence for the formation of Dy^{3+}-doped SrF_2 nanocrystals which causes lowering of nonradiative relaxation of rare-earth ions incorporated into SrF_2 nanocrystals with very low phonon energy [9]. In addition, energy transfer can effectively occur among the neighboring Dy^{3+} ions inside SrF_2 nanocrystals because of the shorter distance between doped ions. The blue emission of the $^4F_{9/2}$–$^6H_{15/2}$ transition is mainly magnetically allowed and insensitive to the crystal field around the ions, whereas the yellow emission of $^4F_{9/2}$–$^6H_{13/2}$ transition is a forced electric dipole transition and allowed only at low symmetries with no inversion center. Dy^{3+} ion can be incorporated in the interior of SrF_2 nanocrystals because the radius of Dy^{3+} ion is smaller than that of SrF_2. However, its site

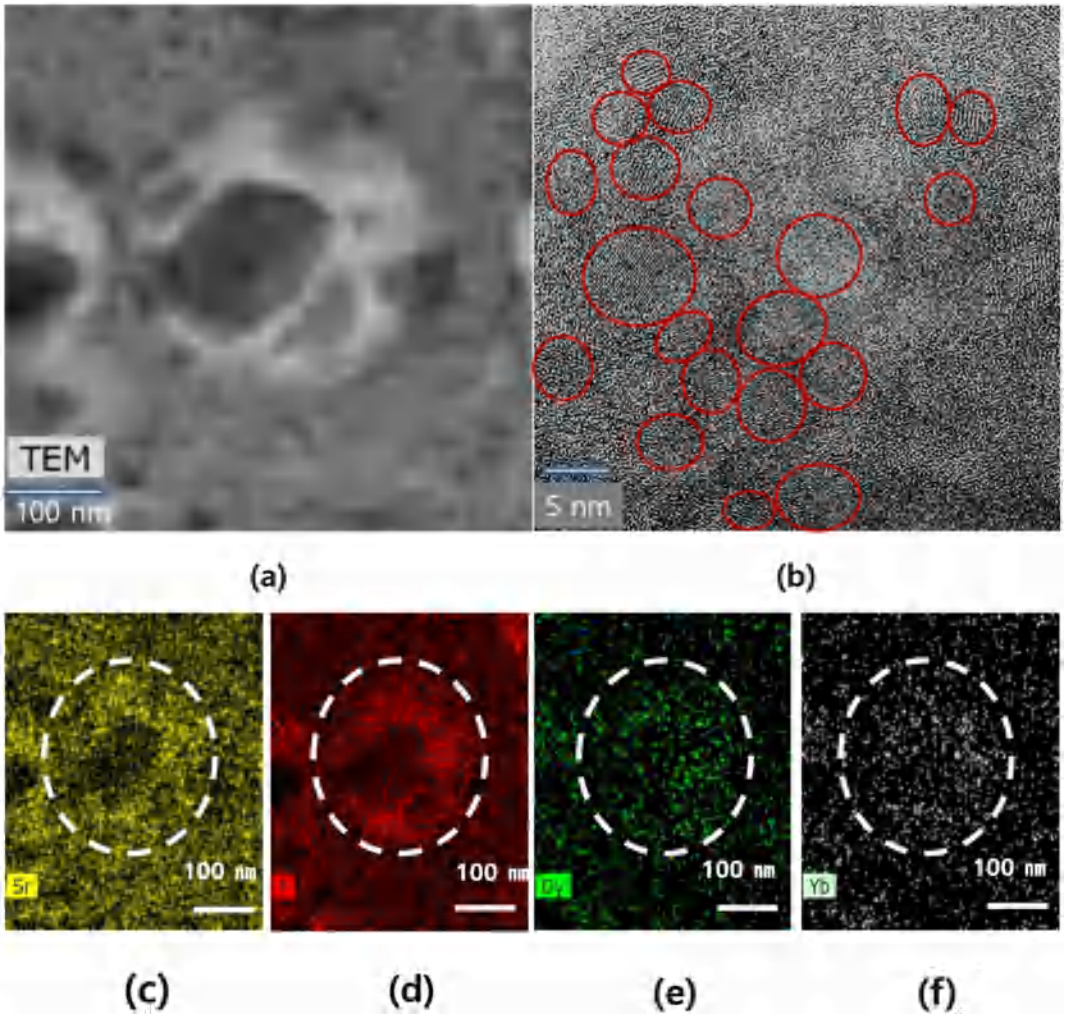

Fig. 2. (a) TEM micrograph of crystallites, (b) HRTEM image of crystalline area, and (c-f) EDS element maps of Sr, F, Dy, and Yb ions in the area of (a) in the GC3 precipitated by CO_2 laser irradiation.

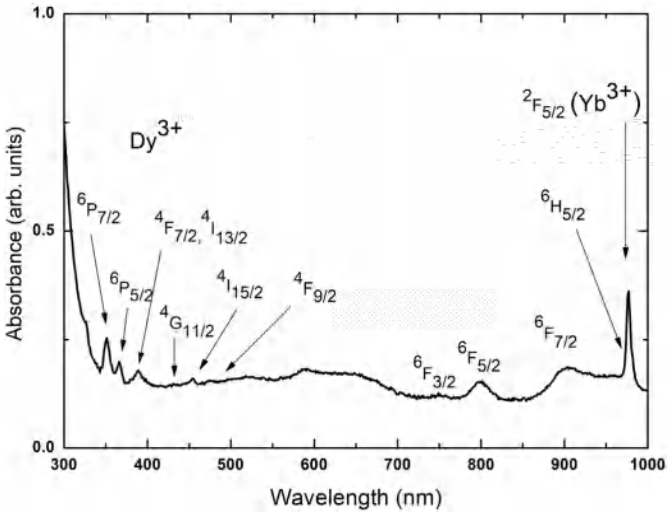

Fig. 3. Absorption spectrum of the as-made glass.

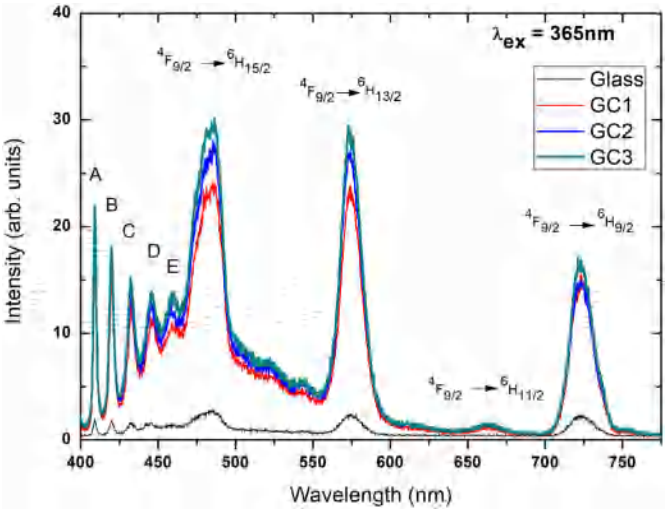

Fig. 4. Down-conversion emission spectra of Dy^{3+} obtained under 365 nm excitation of glass and glass-ceramics. The emissions of A, B, C, D, and E indicate the transitions of $^6P_{7/2}$–$^6H_{13/2}$, $^6P_{5/2}$–$^6H_{11/2}$, $^4G_{11/2}$–$^6H_{15/2}$, $^4I_{13/2}$–$^6H_{13/2}$, and $^4I_{15/2}$–$^6H_{15/2}$ respectively.

symmetry regarding the crystal field may not have inversion symmetry due to a charge compensator which is needed for charge balance, as is the case in CaF_2 [27]. Furthermore, some Dy^{3+} ions can be populated on the surface of SrF_2 nanocrystals, resulting in low site symmetry. Thus, the yellow emission is stronger than the blue emission. The energy level diagram in Fig. 5 shows the possible transitions for the

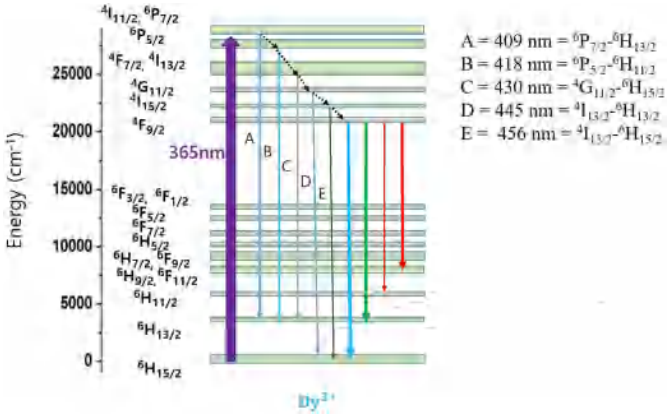

Fig. 5. The energy level diagram to explain the possible transitions for the observed emissions under 365 nm excitation.

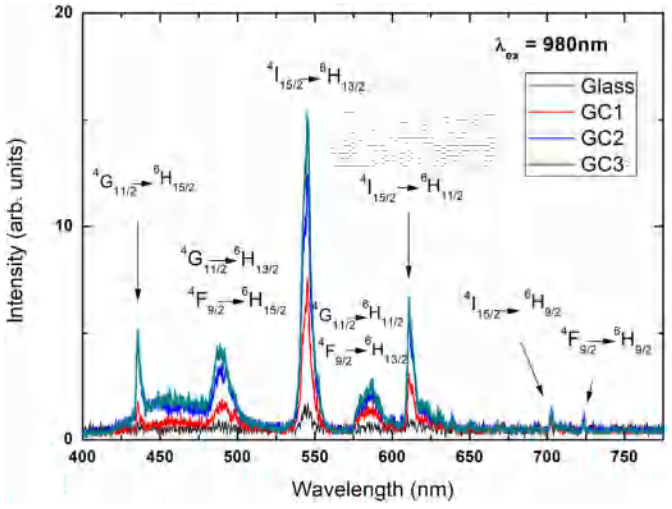

Fig. 6. Upconversion emission spectra of Dy^{3+} obtained under 980 nm excitation of glass and glass-ceramics.

observed emissions under 365 nm excitation.

Upconversion emission spectra of the glass-ceramics obtained under the excitation of the $^2F_{5/2}$ state of Yb^{3+} at 980 nm are shown in Fig. 6. The GC3 produced much stronger visible upconversion emission from the surface, as compared to the as-made glass. The strong upconversion emission from the limited surface region is further evidence for the effective nanocrystal formation. Through the incorporation of Dy^{3+} and Yb^{3+} ions into the SrF_2 crystal phases, the energy transfers can also effectively occur among the neighboring Dy^{3+}–Yb^{3+} ions, because of the shorter distance between doped ions inside nanocrystals. It is well known that the incorporation of Yb^{3+} ions into rare-earth ion doped optical materials is beneficial for infrared-to-visible upconversion emission because Yb^{3+} ions have a strong and broad absorption band around 980 nm. The feature of the upconversion emission spectra is much different from that of the down-conversion spectra in Fig. 4. First, the strongest emission at 542 nm corresponds to the $^4I_{15/2}$–$^6H_{13/2}$ transition. The other emissions of the $^4I_{15/2}$–$^6H_{15/2}$ and $^4I_{15/2}$–$^6H_{11/2}$ transitions also appear at 456 and 610 nm. As shown in Fig. 7, the 980 nm excitation populates both the $^6H_5$ (Dy^{3+}) and $^2F_{5/2}$ (Yb^{3+}) levels, although the $^6H_5$ has a very weak absorption at 980 nm. The electrons reached to the $^6H_{13/2}$ level by nonradiative relaxation from the $^6H_5$ can absorb both the 980 nm pump photons and the transferred energy from the $^2F_{5/2}$ level of Yb^{3+} ion, reaching the $^6F_{1/2}$ level of Dy^{3+} ion. Another absorption process from the $^6F_1$ to the $^4G_{11/2}$, followed by weak emissions of the $^4G_{11/2} \longrightarrow {}^6H_{15/2}$, $^6H_{13/2}$ and $^6H_{11/2}$

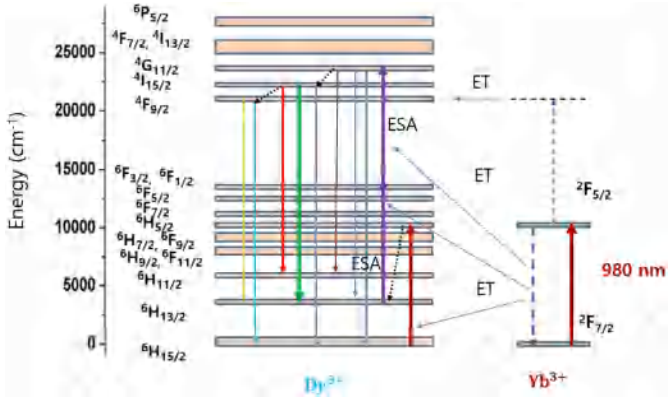

Fig. 7. Energy level diagram of Dy^{3+} and Yb^{3+} ions explaining the main energy transfer processes of Dy^{3+}-Yb^{3+} ions and excited state absorptions in Dy^{3+} ions under 980 nm excitation (ESA: excited state absorption; ET: energy transfer; dot lines: nonradiative relaxations).

transitions. The rapid relaxation from the $^4G_{11/2}$ to $^4I_{15/2}$ level is followed by several emissions from the $^4I_{15/2}$ level, showing the relatively strong emission of the $^4I_{15/2}$–$^6H_{13/2}$ transition. Much of the enhanced emission is due to the crystal environment of Dy^{3+} ions. The nonradiative relaxation from the $^4I_{15/2}$ to $^4F_{9/2}$ level enables the well-known blue and yellow emissions of the $^4F_{9/2}$–$^6H_{15/2}$ and $^4F_{9/2}$–$^6H_{13/2}$ transitions. However, the yellow emission (574 nm) appears to be weaker than the blue emission (483 nm), which differs from the down-conversion in Fig. 4. We must consider the cooperative upconversion emission at 490 nm [28] to explain the difference. The virtual state of Yb^{3+} ions reached by two-step excitation via Yb^{3+}-Yb^{3+} energy transfer produces 490 nm emission, which is transferred to Dy^{3+} ions and overlapped with the blue emission from the $^4F_{9/2}$ level. This implies that the Dy^{3+} site still has non-inversion symmetry.

The band-width of the strongest emission at 542 nm is about 6 nm, which is one-third of the band-width of the yellow or blue band in the down-conversion emission in Fig. 4. The narrower band-width implies that the excited-state absorption and energy transfer are effective only for some subgroups matching the excitation of 980 nm among inhomogeneously distributed sites of Dy^{3+} and Yb^{3+} ions. The main energy transfer channels between Yb^{3+} and Dy^{3+} ions and two excited state absorptions in Dy^{3+} ions are suggested for the blue, green, yellow, and red emissions as displayed in Fig. 7.

4. Conclusions

Dy^{3+}/Yb^{3+} co-doped glass ceramic containing SrF_2 nanocrystals has been prepared by the CO_2 laser surface treatment of $40SiO_2$-$12Al_2O_3$-$23SrF_2$-$24LiF$-$0.5Yb_2O_3$-$0.5Dy_2O_3$ glass. In this glass ceramic, SrF_2 nanocrystals are embedded in the glass matrix and Dy^{3+}/Yb^{3+} ions are incorporated into the SrF_2 nanocrystalline phase. The Dy^{3+} ions in SrF_2 nanocrystals exhibit much enhanced emission intensity, including new emission bands in the 400–460 nm range along with well-known blue and yellow emissions from the $^4F_{9/2}$ level under 365 nm excitation. The upconversion visible emission also showed stronger intensity than the precursor glass under 980 nm excitation, including 430–460 nm blue emission and strong green emission from the $^4I_{15/2}$ level. The substantial enhancement of the emission in glass-ceramics indicates the proper incorporation of Dy^{3+} and Yb^{3+} ions into a nanocrystalline environment. Detailed upconversion mechanisms for the observed emissions are suggested based on the observed emissions. The results may be applied to the patterned white-light imaging technology on the Dy^{3+}-Yb^{3+} co-doped thin glass.

Acknowledgement

This research was supported by Basic Science Research Program through the National Research Foundation of Korea (NRF) funded by the Ministry of Education (2016R1D1A3B03936239).

References

[1] Adam J. Stevenson, Hélène Serier-Brault, Patrick Gredin, Michel Mortier, Fluoride materials for optical applications: single crystals, ceramics, glasses, and glass–-ceramics, J. Fluor. Chem. 132 (2011) 1165–1173.
[2] Matthew J. Dejneka, The luminescence and structure of novel transparent oxyfluoride glass-ceramics, J. Non-Cryst. Solids 239 (1998) 149–155.
[3] F. Lahoz, I.R. Martin, J. Mendez-Ramos, P. Nunez, Dopant distribution in a Tm^{3+}–Yb^{3+} codoped silica based glass ceramic: an infrared-laser induced upconversion study, J. Chem. Phys. 120 (2004) 6180–6190.
[4] Y. Wang, J. Ohwaki, New transparent vitroceramics codoped with Er^{3+} and Yb^{3+} for efficient frequency upconversion, Appl. Phys. Lett. 63 (1993) 3268–3270.
[5] S. Gonzalez-Perez, I.R. Martin, P. Haro-Gonzalez, Local devitrification on an oxyfluoride glass doped with Ho^{3+} ions under argon laser irradiation, Opt. Mater. 31 (2009) 1373–1375.
[6] J.-P.R. Wells, R.J. Reeves, Upconversion fluorescence of Eu^{3+} doped alkaline earth fluoride crystals, J. Lumin. 66 (67) (2004) 219–223.
[7] Xvsheng Qiao, Xianping Fan, Jin Wang, Minquan Wang, Luminescence behavior of Er^{3+} in glass-ceramics containing CaF_2 nanocrystals, J. Non-Cryst. Solids 351 (2005) 357–363.
[8] Radosław Lisiecki, Elz_bieta Augustyn, Witold Ryba-Romanowski, Michal Zelechower, Er-doped and Er, Yb co-doped oxyfluoride glasses and glass–-ceramics, structural and optical properties, Opt. Mater. 33 (2011) 1630–1637.
[9] L.A. Riseberg, H.W. Moos, Multiphonon orbit-lattice relaxation of excited states of rare-earth ions in crystals, Phys. Rev. 174 (1968) 429–438.
[10] M. Secu, C.E. Secu, S. Polosan, G. Aldica, C. Ghica, Crystallization and spectroscopic properties of Eu-doped CaF_2 nanocrystals in transparent oxyfluoride glass-ceramics, J. Non-Cryst. Solids 355 (2009) 1869–1872.
[11] S.E. Mekhlouf, A. Boukenter, M. Ferrari, F. Goutaland, N. Ollier, Y. Ouerdane, UV assisted local crystallization in Er^{3+} doped oxy-fluoride glass, J. Non-Cryst. Solids 353 (2007) 506–509.
[12] M. Kusatsugu, M. Kanno, T. Honma, T. Komatsu, Spatially selected synthesis of LaF_3 and Er^{3+}-doped CaF_2 crystals in oxyfluoride glasses by laser-induced crystallization, J. Solid State Chem. 181 (2008) 1176–1183.
[13] V.P. Veiko, G.K. Kostyuk, N.V. Nikonorov, E.B. Yakovlev, Structural phase modification of glass-ceramic materials under CO_2 laser irradiation, Bull. Russ. Acad. Sci. Phys. 72 (2008) 167–171.
[14] Daqin Chen, Yuansheng Wang, En Ma, Yunlong Yu, Feng Liu, Partition, luminescence and energy transfer of Er^{3+}/Yb^{3+} ions in oxyfluoride glass ceramic containing CaF_2 nano-crystals, Opt. Mater. 29 (2007) 1693–1699.
[15] Su-A Song, Dong-Seon Kim, Hong-Myeong Jeong, Ki-Soo Lim, Upconversion in Nd–Tm–Yb triply doped oxyfluoride glass–ceramics containing CaF_2 nanocrystals, J. Lumin. 152 (2014) 75–78.
[16] A. Santana-Alonso, J. Méndez-Ramos, A.C. Yanes, J. del-Castillo, V.D. Rodríguez, Up-conversion in sol–gel derived nano-glass–ceramics comprising $NaYF_4$ nanocrystals doped with Yb^{3+}, Ho^{3+} and Tm^{3+}, Opt. Mater. 32 (2010) 903–908.
[17] E.V. Vilejshikova, P.A. Loiko, G.E. Rachkovskaya, G.B. Zakharevich, K.V. Yumashev, Up-conversion luminescence in oxyfluoride glass-ceramics with PbF_2:(Yb^{3+}, Eu^{3+}, RE^{3+}) (RE = Tm, Ho, or Er) nanocrystals, J. Appl. Spectrosc. 83 (2016) 723–729.
[18] Qiu Jianbei, Jiao Qing, Zhou Dacheng, Yang Zhengwen, Recent progress on upconversion luminescence enhancement in rare-earth doped transparent glass-ceramics, J. Rare Earths 34 (2016) 341–367.
[19] Linlin Liu YanminYang, Shuzhen Cain, Fuyun Jiao, Chao Mi, Xianyuan Su, Jiao Zhang, Fang Yu, Xiaodong Li, Ziqiang Li, Up-conversion luminescence and near-infrared quantum cutting in Dy^{3+}, Yb^{3+} co-doped $BaGd_2ZnO_5$ nanocrystal, J. Lumin. 146 (2014) 284–287.
[20] Hao Dong, Ling-Dong Sun, Chun-Hua Yan, Energy transfer in lanthanide upconversion studies for extended optical applications, Chem. Soc. Rev. 44 (2015) 1608–1634.
[21] Weiwei Li, Bingchu Mei, Jinghong Song, Zhe Wang, Fabrication and optical property of highly transparent SrF_2 ceramic, Mater. Lett. 159 (2015) 210–212.
[22] A.L. Patterson, The Scherrer formula for x-ray particle size determination, Phys. Rev. 56 (1939) 978–981.
[23] Masaki Kanno, Tsuyoshi Honma, Takayuki Komatsuw, Two-dimensional mapping of Er^{3+} photoluminescence in CaF_2 crystal lines patterned by lasers in oxyfluoride glass, J. Am. Ceram. Soc. 92 (2009) 825–829.
[24] Mohammad Hassan Imanieh, Bijan Eftekhari Yekta, V. Marghussian, Saeed Shakhesi, I.R. Martín, Crystallization of nano calcium fluoride in CaF_2-Al_2O_3-SiO_2 system, Solid State Sci. 17 (2013) 76–82.
[25] O. Ravi, C. Madhukar Reddy, B. Sudhakar Reddy, B. Deva Prasad Raju, Judd–Ofelt analysis and spectral properties of Dy^{3+} ions doped niobium containing tellurium calcium zinc borate glasses, Opt. Commun. 312 (2014) 263–268.
[26] Ying Fang, Weidong Zhuang, Yunsheng Hua, Xinyu Ye, Xiaowei Huang, Luminescent properties of Dy^{3+} ion in $Ca_8Mg(SiO_4)_4Cl_2$, J. Alloys Compd. 455 (2008) 420–423.
[27] Qun Luo, Xvsheng Qiao, Xianping Fan, Shiqi Liu, Hui Yang, Xianghua Zhang, Reduction and luminescence of europium ions in glass ceramics containing SrF2 nanocrystals, J. Non-Cryst. Solids 354 (2008) 4691–4694.
[28] Xiuhong Pan, Jianding Yu, Yan Liu, Shinichi Yoda, Minghui Zhang, Fei Ai, Fei Jin, Huimei Yu, Weiqing Jin, Infrared to visible upconversion luminescence in Er^{3+}/Yb^{3+} doped titanate glass prepared by containerless processing, J. Lumin. 132 (2012) 1025–1029.